Systematic analysis of heavy-ion reaction data in terms of an eikonal approach: Elastic and inelastic scattering

S. M. Lenzi
Dipartimento di Fisica and Istituto Nazionale di Fisica Nucleare, Padova, Italy
and Consejo Nacional de Investigaciones Científicas y Tecnicas, Buenos Aires, Argentina

A. Vitturi
Dipartimento di Fisica and Istituto Nazionale di Fisica Nucleare, Trento, Italy

F. Zardi
Dipartimento di Fisica and Istituto Nazionale di Fisica Nucleare, Padova, Italy
(Received 11 May 1989)

An approximation to the Glauber model for heavy-ion scattering has been recently derived and illustrated by a few examples in two previous papers. We present here a more systematic analysis of nucleus-nucleus elastic and inelastic scattering data, which cover a wide range in the projectile energy ($E/A_P \approx 30-350$ MeV), the mass number of colliding nuclei ($4 \leq A_P \leq 40$, $12 \leq A_T \leq 208$), and the multipolarities of the excited states. The only inputs of the model are the densities and transition densities of the nuclei and the elementary nucleon-nucleon scattering amplitudes, which have been taken from the current literature without any adjustment. The results obtained are in overall good agreement with the experimental data.

I. INTRODUCTION

In the last few years a large amount of experimental data has become available in the field of heavy-ion grazing collisions at intermediate energies, such as elastic and inelastic scattering, stripping and pickup reactions, and spin and isospin exchange.

At low bombarding energies the grazing collisions are usually described in the framework of the optical model and distorted-wave Born approximation (DWBA) or coupled-channels (CC) formalism.[1] In those approaches the internal degrees of freedom and the ones pertaining to the scattering process are strongly mingled, so that it is not always easy to separate their effects and to state their relative importance.

On the converse, reactions induced by light ions at very high energy are well described by resorting to the Glauber model and to its so-called optical limit. It is assumed in these models that all the dynamics of the scattering process is dominated by nucleon-nucleon collisions. The only ingredients for these descriptions are the densities and transition densities of the colliding nuclei and the elementary N-N scattering amplitudes. Owing to its appealing simplicity, it is clearly worth assessing the applicability of this method to intermediate-energy heavy-ion scattering processes.

A systematic and successful analysis of the nucleus-nucleus total reaction cross section, including bombarding energies of few MeV per nucleon, has been carried out by Di Giacomo, De Vries, and Peng[2] in the above scheme. Though the total reaction cross section is a rather simple quantity, these achievements may also be viewed as a suggestion to exploit the possibilities of the Glauber method in more complicated heavy-ion scattering processes also at intermediate energies. In a previous paper we proposed a completely microscopic formulation of the optical limit to describe heavy-ion elastic scattering[3] and then extended the formalism to the description of inelastic scattering[4] (by "microscopic" we mean that both the projectile and the target are considered as formed by nucleons, at variance with semimicroscopic approaches in which the projectile is treated as an extended body without internal degrees of freedom[5,6]). To test the efficiency of the model, a few examples of fit of experimental data at relatively low bombarding energy ($E/A = 20-100$ MeV) were given. In the present paper a larger amount of experimental data is considered, which covers wider regions in energy, mass number of the colliding nuclei, and multipolarities of excited states. A forthcoming paper will be devoted to the analysis of charge exchange reactions, which cannot be described in semimicroscopic approaches, since the reaction induces transitions in both target and projectile. The scheme of the extension of this formalism for the description of such reactions is given in Ref. 7.

We stress the importance of a correct description of the elastic scattering as a necessary prerequisite for the analysis of heavy-ion scattering experiments. In fact, most heavy-ion collisions can be described either as perturbative processes on a background of elastic diffusion, as the grazing reactions, or as relying heavily on the elastic transmission coefficients, as is the case of fusion reactions. In this connection it is worthwhile to emphasize that the model gives an overall good account of the elastic data, although the variety of cases considered displays very different behaviors of the angular distributions, ranging from the Fraunhofer diffractive patterns characteristic of the scattering with light targets to the

rainbow-shaped cross sections arising from heavy target scattering.

The paper is organized as follows. We start by giving a brief review of the formalism in Sec. II. The applications to elastic and inelastic processes are presented in Secs. III and IV, respectively. A brief final comment is given in Sec. V.

II. THE FORMALISM

Different derivations of the optical limit to the Glauber model have been carried out in the literature. The original and standard derivation[8,9] assumes as a starting point a version of the Glauber model in which the correlations among the nucleons are neglected. As further conditions, one takes the limit of a large number of particles, with mass numbers of projectile and target and elementary nucleon-nucleon cross sections satisfying the relations $A_P A_T \to \infty$ and $A_P A_T \sigma_{NN} \to$ const. Within this framework the optical limit appears therefore as an approximation to the uncorrelated Glauber model.

One must observe, however, that at rather low bombarding energies the optical limit turns out to work better than the uncorrelated Glauber model itself, a situation also encountered at high energy for light colliding nuclei such as $\alpha + {}^{12}\mathrm{C}$.[7,10] This paradox can be explained by observing that an alternative derivation of the optical limit can be obtained (see, e.g., Refs. 4, 5, 7, 10, and 11) from the Glauber model by a method in which the hypothesis of absence of correlations plays no role. On this ground one can state that the optical limit and the uncorrelated Glauber model are two independent approximations to the correlated Galuber model, with possible different ranges of validity.

We only need to recall here the final form assumed by the elastic and inelastic scattering amplitudes, addressing the reader to Ref. 4 for derivations and discussions. We start defining the nucleon-nucleon scattering amplitude $f_{NN}(q)$ and the related profile, connected by the Fourier transform

$$\gamma(b)=\frac{1}{2\pi i k_{NN}}\int d^2q\, e^{-i\mathbf{q}\cdot\mathbf{b}} f_{NN}(q)\ . \tag{1}$$

The variable b is the impact parameter and k_{NN} is the nucleon-nucleon relative momentum in the center-of-mass (c.m.) system. The basic quantity $\lambda(b)$ entering in the optical limit is the "elementary phase shift," defined by the relation

$$\begin{aligned}\lambda(b)&=\int \rho_0^P(\mathbf{r}_P)\rho_0^T(\mathbf{r}_T)\gamma(\mathbf{b}-\mathbf{s}_P-\mathbf{s}_T)d\mathbf{r}_P d\mathbf{r}_T\\&=\frac{1}{2\pi i k_{NN}}\int \hat{\rho}_0^P(q)\hat{\rho}_0^T(q) f_{NN}(q) e^{-i\mathbf{q}\cdot\mathbf{b}} d\mathbf{q}\ .\end{aligned} \tag{2}$$

In the preceding expression we introduced the densities $\rho_0^T(\mathbf{r})$ and $\rho_0^P(\mathbf{r})$ of the target and the projectile [normalized so that $\int \rho_0^{T,P}(\mathbf{r})d\mathbf{r}=1$] and their Fourier transform $\hat{\rho}_0^{T,P}(q)$. The label "0" stands for the ground state. The projections of the coordinate vectors on the plane perpendicular to the incident momentum are denoted $\mathbf{s}_P$ and $\mathbf{s}_T$. In terms of $\lambda(b)$ the elastic scattering amplitude is written in the form

$$\begin{aligned}f_{00}(\Delta)&=ik\int db\, bJ_0(\Delta b)\{1-[1-\lambda(b)]^{A_T A_P}\}\\&\approx ik\int db\, bJ_0(\Delta b)(1-e^{-A_T A_P \lambda(b)})\ ,\end{aligned} \tag{3}$$

where k and Δ are the nucleus-nucleus momentum and transferred momentum in the c.m. system.

Similar formulae apply to the inelastic scattering processes. Let us consider the excitation of a target state with quantum numbers LM. Our model description of the process assumes that the transition to the excited state is originated at any scattering order by one elementary collision, all the others being of elastic character. In this scheme one obtains the inelastic differential cross section for the nucleus-nucleus collision in the form[4]

$$\begin{aligned}(d\sigma/d\omega)_L&=\sum_{M=-L}^{L}\left|kA_TA_P\int_0^\infty db\, bJ_M(qb)\mu_{LM}(b)[1-\lambda(b)]^{A_TA_P-1}\right|^2\\&\approx\sum_{M=-L}^{L}\left|kA_TA_P\int_0^\infty db\, bJ_M(qb)\mu_{LM}(b)e^{-\lambda(b)A_TA_P}\right|^2,\end{aligned} \tag{4}$$

where

$$\mu_{LM}(b)=\frac{1}{ik}B_{LM}\int_0^\infty dq\, q\hat{\rho}_0^P(q)f_{NN}(q)\hat{\rho}_L^T(q)J_M(qb) \tag{5}$$

with

$$B_{LM}=(-1)^M\left[\frac{2L+1}{4\pi}\right]^{1/2}\frac{[(L-M)!(L+M)!]^{1/2}}{(L-M)!!(L+M)!!}\times\left[\frac{1+(-1)^{L+M}}{2}\right]. \tag{6}$$

The nondiagonal kernels $\mu_{LM}(b)$ can be interpreted as an eikonalized form factor involving the Fourier transform

$$\hat{\rho}_L^T(q)=4\pi\int dr[r^2 j_L(qr)\rho_L^T(r)] \tag{7}$$

of the transition density associated with the excitation of the state $|LM\rangle$ of the target

$$\rho_{LM}^T(\mathbf{r})=\rho_L^T(r)Y_{LM}(\hat{r})\ . \tag{8}$$

It may be worthwhile noticing that expression (4) for the inelastic cross section can assume, with some additional approximations, the familiar form obtained in the impulse approximation.

Different models can of course be advanced for the transition densities (see, e.g., Chap. 14 of Ref. 1). Leaving aside microscopic constructions of the transition densities based on random-phase approximation (RPA) calculations, in most applications to collective states of vi-

brational character one has resorted to models based on the surface macroscopic variables. In this context common choices are the transition densities obtained in the Tassie model

$$\rho_L^T(r)=\frac{\beta_L}{\sqrt{2L+1}}r\left[\frac{r}{R_T}\right]^{L-2}\frac{d\rho_0^T(r)}{dr} \tag{9}$$

and in the Bohr-Mottelson model

$$\rho_L^T(r)=\frac{\beta_L R_T}{\sqrt{2L+1}}\frac{d\rho_0^T(r)}{dr}\ , \tag{10}$$

both models expressing the transition density in terms of the ground-state nuclear density. As one can see, for the excitation of states of multipolarity $L=2$ the two functions assume at the nuclear surface the same value, while different behaviors are expected for higher multipolarities. Examples of the sensitivity of the results to the choice of the transition densities will be discussed in the applications in Sec. IV.

We have to reserve a comment to the assumption of straight-line propagation. This hypothesis is not adequate for heavily charged nuclei at relatively low bombarding energies, where the deviations of the Rutherford orbits from the straight line are also marked for grazing partial waves. The neglect of the Coulomb focusing effect leads to an overestimation of the value of the grazing angular momentum and consequently to an incorrect description of the angular distributions. As suggested in Ref. 3, our simple prescription for overcoming this problem is to evaluate all elastic and inelastic integrals for each partial wave l not in correspondence to the asymptotic impact parameter b but to the associated distance of closest approach in Rutherford orbits b', i.e.,

$$kb'=\eta+(\eta^2+k^2b^2)^{1/2}\ , \tag{11}$$

η being the Sommerfeld parameter.

Further comments deserve the inclusion of the contribution of the Coulomb field to the elastic and inelastic amplitudes and the description of strongly-coupled situations. The treatment of long-ranged interactions within a microscopic model based on N-N collisions is not immediate. As an operative prescription we added to the Glauber elastic phase shift the high-energy approximation to the Coulomb phase shift in the form

$$\sigma_c(b)=\eta\ln kb\ , \tag{12}$$

while the contribution of the Coulomb excitation to the inelastic scattering amplitude has not been included. On the converse, strongly coupled situations which need a description in terms of a sequence of back and forth transitions, can be naturally included in our formalism, here restricted to only one microscopic collision of inelastic character. Preliminary developments along this line can be found in Ref. 7.

III. ELASTIC SCATTERING

Within the formalism recalled in the previous section we have analyzed the elastic scattering for a set of heavy-ion reactions. The variety of the situations encountered can be underlined by noting that the collision energy ranges form 30 to 350 MeV per nucleon. In addition, the product of the mass numbers of the colliding nuclei, a parameter which is relevant in an approach that describes the global process in terms of microscopic collisions, ranges from 48 to 4160

It is worthwhile to note that in our previous calculations (Refs. 3 and 4) Gaussian shapes were used as a parametrization of the nuclear densities. For heavy nuclei this was done by restoring to a prescription by Karol[12] which amounts to using Gaussian distributions which fit the actual densities in the surface region. The advantage of using Gaussian distributions is that they allow for an analytical treatment of most of the calculations to be carried out. It emerges from the analyses put forward in the present work that for higher energies and/or lighter projectiles the nuclei become rather transparent to each other. We have therefore preferred to use realistic density distributions throughout, at the price of slightly more involved computations. The parameters describing the nuclear densities are given in Table I, while those associated with the elementary scattering amplitudes are given in Table II. These parametrizations lead directly to the results shown in Figs. 1–9 for the different reactions.

TABLE I. Density parameters. The nuclear densities are described using the following models: Gaussian, $\rho(r)=\rho(0)e^{-r^2/a^2}$; modified Fermi (MF), $\rho(r)=\rho(0)(1+wr^2c^2)/(1+e^{(r-c)/z}$; modified Gaussian (MG), $\rho(r)=\rho(0)(1+wr^2/c^2)/(1+e^{(r^2-c^2)/z^2})$.

Nucleus	Model	c or a (fm)	z (fm)	ω	Reference
^{4}He	Gaussian	1.37			24
^{12}C	MF	2.335	0.5224	−0.149	24
^{16}O	MF	2.608	0.513	−0.051	24
^{20}Ne	MF	2.74	0.569	0	24
^{28}Si	MF	3.30	0.545	−0.018	24
^{40}Ca	MF	3.725	0.591	−0.169	24
^{42}Ca	MF	3.627	0.594	−0.102	25
^{58}Ni	MF	4.309	0.517	−0.1308	24
^{90}Zr	MG	4.522	2.5216	0.245	24
^{208}Pb	MF	6.624	0.549	0	24

TABLE II. Parameters of the nucleon-nucleon amplitude. The amplitude is considered isotropic up to 120 MeV: $f_{NN}=[k_{NN}\sigma_{NN}(i+\alpha_{NN})]/4\pi$. For higher energies we used the form $f_{NN}(q)=f_{NN}e^{-aq^2/2}$.

E/A (MeV/u)	σ_{NN} (fm^2)	α_{NN}	a (fm^2)
30	19.6	0.87	
38	14.6	0.89	
40	13.5	0.9	
49	10.4	0.94	
85	6.1	1	
94	5.5	1.07	
120	4.5	0.7	
200	3.2	0.6	0.02
342.5	2.84	0.26	0.045

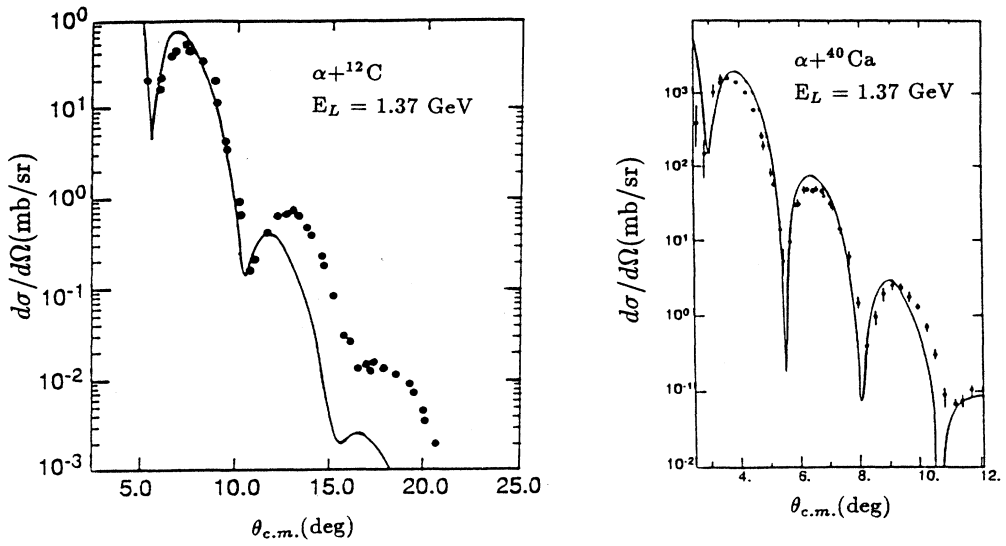

FIG. 1. Elastic cross section of 1.37 GeV α particles on ^{12}C and ^{40}Ca. Experimental data are taken from Refs. 17 and 18, respectively.

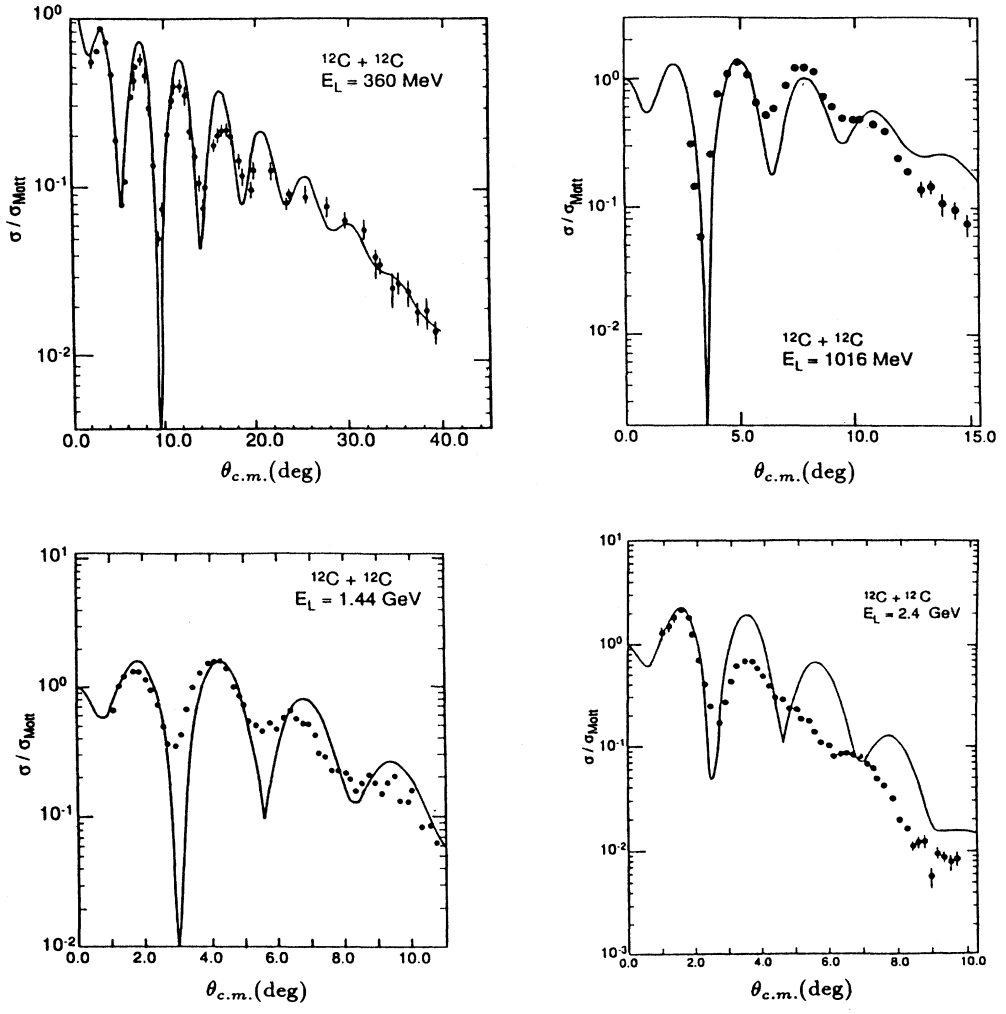

FIG. 2. Elastic angular distribution for the $^{12}C+^{12}C$ reaction at 360, 1016, 1440, and 2400 MeV. The experimental data are taken from Refs. 19 and 14.

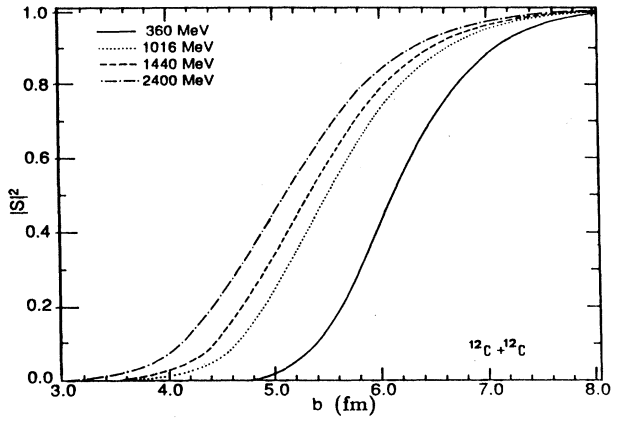

FIG. 3. Transmission factors for the $^{12}C+^{12}C$ reaction at 360, 1016, 1440, and 2400 MeV.

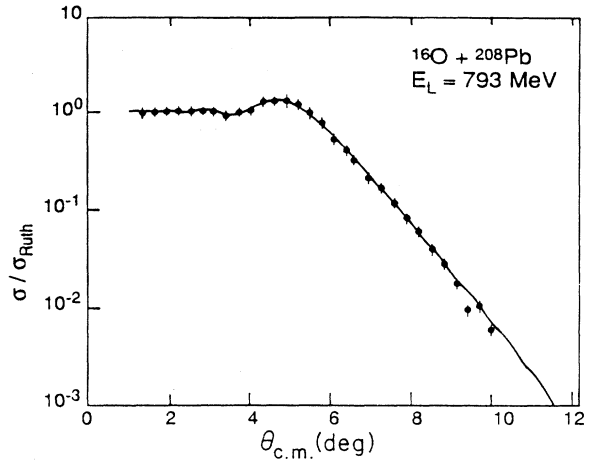

FIG. 5. Elastic angular distribution for the $^{16}O+^{208}Pb$ reaction at 793 MeV. The experimental data are taken from Ref. 20.

Before commenting in some more detail on the different systems, one can immediately observe that the reproduction of the data is very good in the whole available angular range for most of the collisions analyzed. This wide-range angular fit is particularly remarkable since the approach, based on the eikonal assumption, is only expected to work at very forward scattering angles. The only exception to this overall positive picture seems to be offered, as discussed later, by the reactions involving ^{12}C at rather high energies.

A clear first example of the preceding statement can be already found in Fig. 1, which refers to the scattering of α particles. The calculation shows an excellent fit to the elastic angular distribution in the case of the ^{40}Ca target, while for the ^{12}C case the agreement is confined to the angular range up to $\approx 12°$. For larger angles, in fact, although the position of maxima and minima are correct, the magnitude of the cross section is underestimated. We should note that the same kind of difficulties were present within the Glauber model in other calculations involving ^{12}C, and no improvement was obtained by resorting to the use of different profiles for the *n-p*, *p-p*, and *p-n* scattering.[13]

We turn now to the collision $^{12}C+^{12}C$ at different bombarding energies. The predicted angular distributions are shown in Fig. 2. For the two higher energies only the forward angular region, corresponding to the peripheral part of the collision, is well reproduced, while for larger angles just the qualitative trend is accounted for. Good results for the whole angular range are instead obtained for the cases corresponding to lower bombarding energies. This behavior with the energy is apparently at odds with our expectation of a general improvement with increasing energy. One should keep in mind, however, that as the corresponding nucleon-nucleon collision energy approaches the value associated with the minimum of

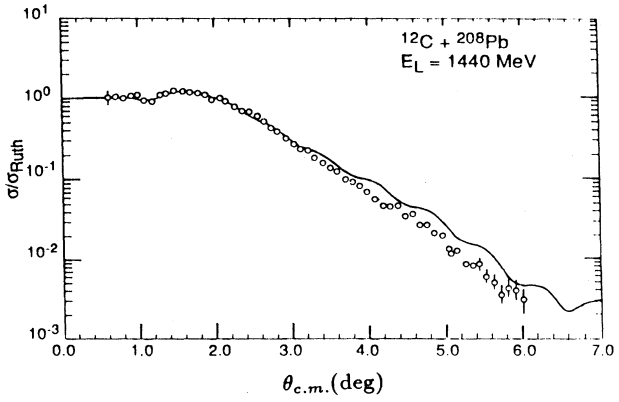

FIG. 4. Elastic angular distribution for the $^{12}C+^{208}Pb$ reaction at 1440 MeV. The experimental data are taken from Ref. 14.

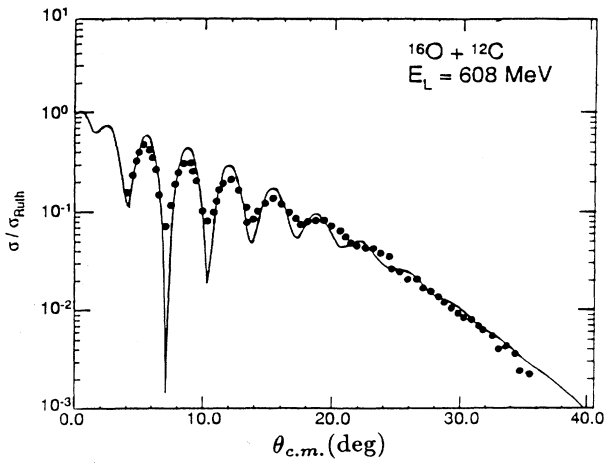

FIG. 6. Elastic angular distribution for the $^{16}O+^{12}C$ reaction at 608 MeV. The experimental data are taken from Ref. 15.

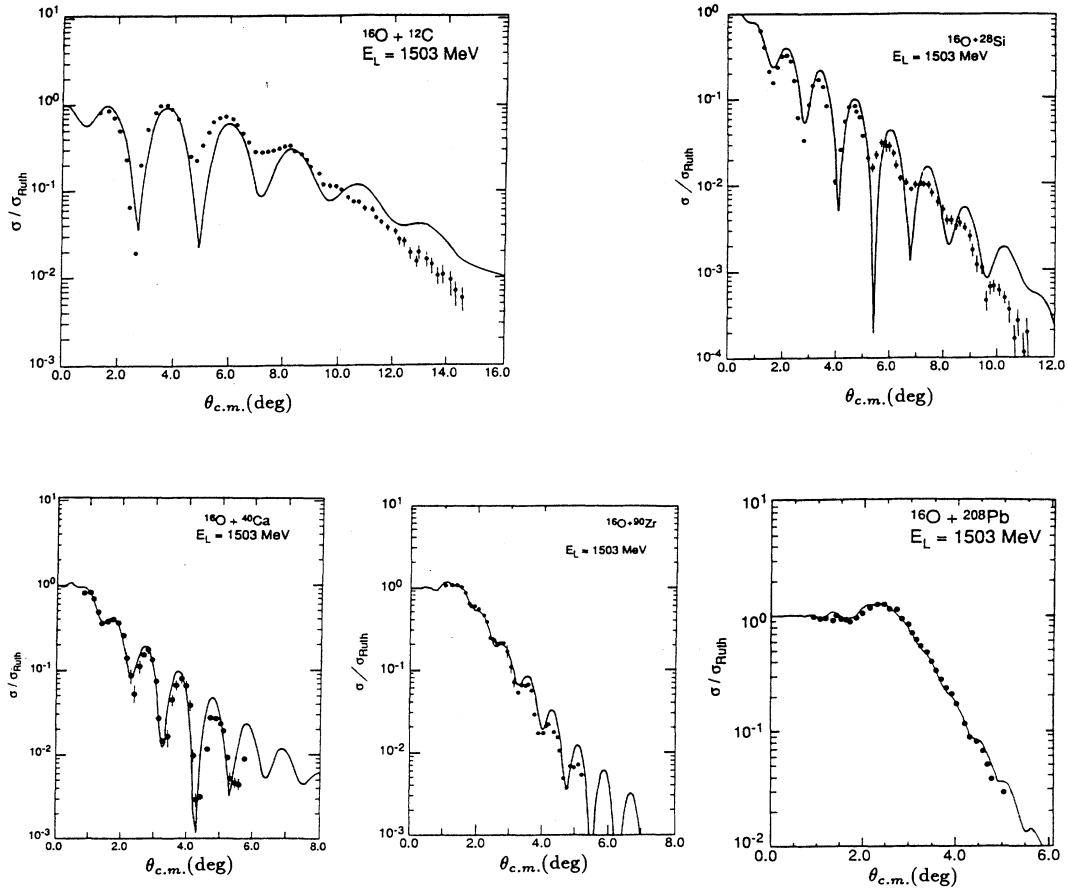

FIG. 7. Elastic angular distributions for the scattering of ^{16}O on ^{12}C, ^{28}Si, ^{40}Ca, ^{90}Zr, and ^{208}Pb at 1503 meV. The experimental data are taken from Ref. 21.

σ_{NN}, i.e., $E/A \approx 250$ MeV, we obtain an increase of the nuclear transparency, as evidenced by the transmission coefficients displayed in Fig. 3 for the different energies. This suggests that, although the eikonal approximation becomes more and more precise at higher energies, the larger transparency increases the sensitivity to the internal part of the nuclear couplings. In this situation a coupled-channel treatment would be more adequate. Otherwise stated, the frozen nuclei hypothesis in which the optical limit has been deduced[4] is not valid for strong overlapping of the density distributions. We have to point out that fits of better quality were obtained within an optical-model search.[14] In the same reference however, a parameter free analysis was also attempted, using an optical-model potential as derived in lowest order from the Goldberger-Watson multiple scattering theory, supplemented by corrections due to the Fermi motion and Pauli correlations. Although this latter approach is somewhat more sophisticated than ours, the kind of agreement with the experimental data is practically equivalent.

Good results are obtained for the cases of the reactions $^{12}C+^{208}Pb$ at 1440 MeV (Fig. 4), $^{16}O+^{208}Pb$ at 793 MeV (Fig. 5), and $^{16}O+^{12}C$ at 608 MeV (Fig. 6), a case that has raised a particular interest,[15] for the peculiarity of the angular distribution which displays a Fraunhofer diffraction followed by a smooth decaying tail.

Particularly significative are the analyses of the scattering data of ^{16}O colliding with different targets at the fixed energy of 1503 (Fig. 7). As the mass of the target increases, the cross section develops continuously from a Fraunhofer shape to a characteristic rainbow shape. The same behavior of the cross sections can be observed for reactions induced by ^{12}C at 1030 MeV on several targets (Fig. 8). While for the first series with ^{16}O projectiles the agreement between experiment and theoretical predictions is quite good both in shape and magnitude, results of somewhat lower quality are obtained in the case of ^{12}C projectiles.

We have also analyzed ^{20}Ne induced reactions on both ^{90}Zr and ^{208}Pb target (Fig. 9). In this case effects due to the distortion of ^{20}Ne are expected to play some role. To complete this survey we finally recall the good fit obtained in our previous paper[3] for the reactions $^{13}C+^{208}Pb$ at 390 MeV and $^{40}Ar+^{208}Pb$ at 1760 MeV.

The general trend is therefore that, as far as the elastic

scattering is concerned, the model seems to incorporate all the relevant degrees of freedom of the process, with results that are qualitatively and quantitatively similar to those obtained in the usual optical-model description. Although they are different, the two approaches should have a correspondence, and it is obvious to try to compare the fitted optical-model potential with that obtained by inversion procedure from the Glauber elastic phase shifts

$$\delta(b)=\frac{1}{2i}A_T A_P \lambda(b) .$$

This can be calculated within the eikonal approximation through the Abel transform

$$V(r)=\frac{2\hbar v}{\pi r}\frac{d}{dr}\int_r^\infty \frac{\delta(b)}{(b^2-r^2)^{1/2}} r\,dr . \tag{13}$$

The procedure was tested in Ref. 3, leading to effective potentials which on the tail, where the process takes place, are very close to those obtained by fitting the experimental data. It can also be analytically proved that under certain approximations, and for Gaussian density distributions, the potential obtained through Eq. (13) coincides with that obtained by the double folding procedure.

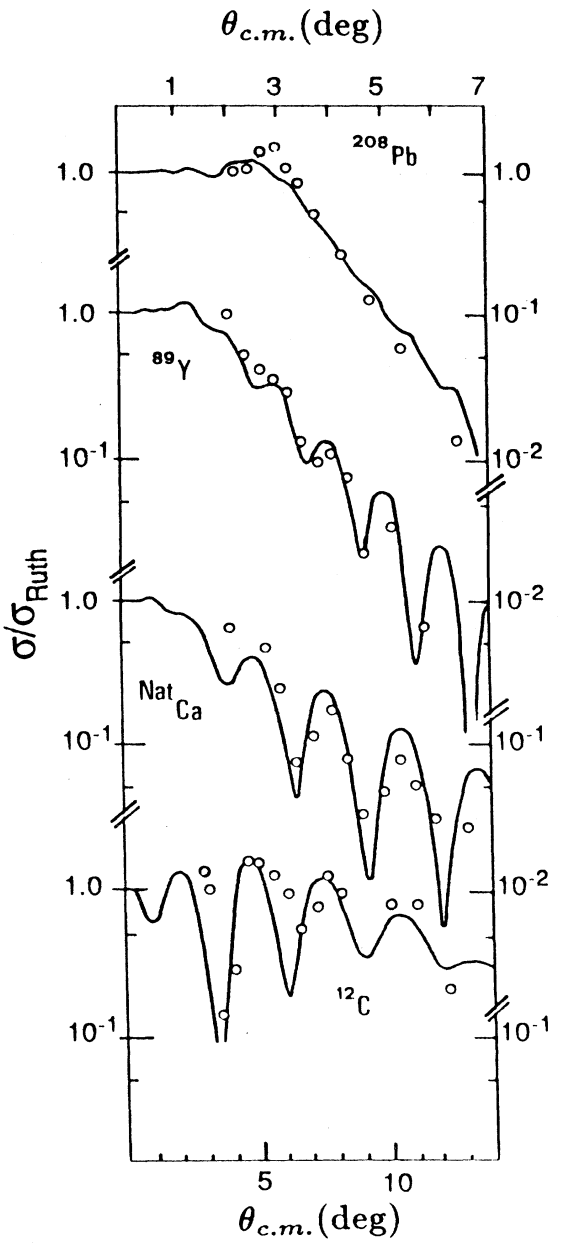

FIG. 8. Elastic angular distributions for the scattering of ^{12}C on ^{12}C, ^{Nat}Ca, ^{89}Y, and ^{208}PB at 1.03 GeV. The lower horizontal scale corresponds to the ^{12}C data; for all the other targets the angle must be read on the upper scale (which is half the lower scale). In the fit to ^{Nat}Ca we have assumed that the target is ^{40}Ca. The experimental data are taken from Ref. 22.

IV. INELASTIC SCATTERING

We move now to the analysis of inelastic scattering data. The parameters used for the densities and N-N amplitudes are the same used for the elastic scattering analyses (Tables I and II). The deformation parameters entering in the transition densities have been obtained from the experimental $B(E,L)$ values and are given in the captions to the figures. We have already pointed out that a crucial role for a proper description of the reaction channels is played by the elastic scattering. We cannot therefore expect improvement of the quality of the fits over that displayed by the corresponding elastic cross section.

The first example of this statement is offered by the comparison of the inelastic excitation of the first 2^+ state in ^{12}C, ^{42}Ca, and ^{58}Ni induced by α particles of 1.37 GeV bombarding energy (Fig. 10). The first two cases should be compared with the corresponding elastic scattering process given in Fig. 1. While the quality of the agreement is good in all the angular range for ^{42}Ca and ^{58}Ni, in the case of ^{12}C it is only satisfactory in the forward region, in clear correspondence with the elastic case.

A similar effect holds for the $^{12}C+^{12}C$ reaction exciting the 2^+ state at 4.4 MeV for the set of energies already considered for the elastic scattering. The angular distributions corresponding to the two higher bombarding energies are displayed in Fig. 11, while those corresponding to the lower energies can be found in Ref. 4. As in the elastic scattering case (cf. Fig. 2), the agreement with the experimental data is better for the lower energies.

In the preceding cases, all referring to the excitation of 2^+ states, no detectable difference could be obtained by using the Tassie or the "standard" model. Differences, on the other hand, arise for higher multipolarities. This is exemplified in Fig. 12, where we consider the excitation of the 3^- and 5^- states in ^{40}Ca by α particles. In both cases the angular distributions obtained by making use of the "standard" model present a clearly better fit than those of the Tassie model. This conclusion is in full

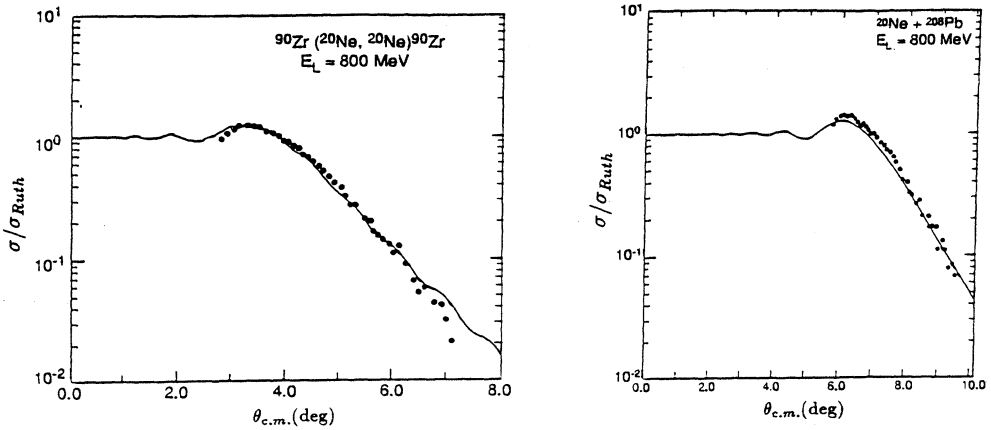

FIG. 9. Elastic angular distribution for the scattering of ^{20}Ne on ^{90}Zr and ^{208}Pb at 800 MeV. The experimental data are taken from Ref. 23.

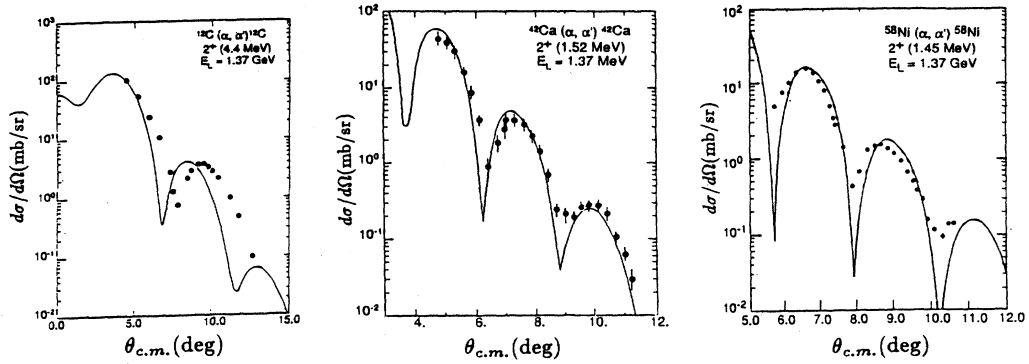

FIG. 10. Inelastic angular distributions of 1.37 GeV α particles exciting the first 2^+ states of ^{12}C, ^{42}Ca, and ^{58}Ni. The deformation parameters β_2 used are 0.4, 0.21, and 0.2, respectively. The experimental data are taken from Ref. 6.

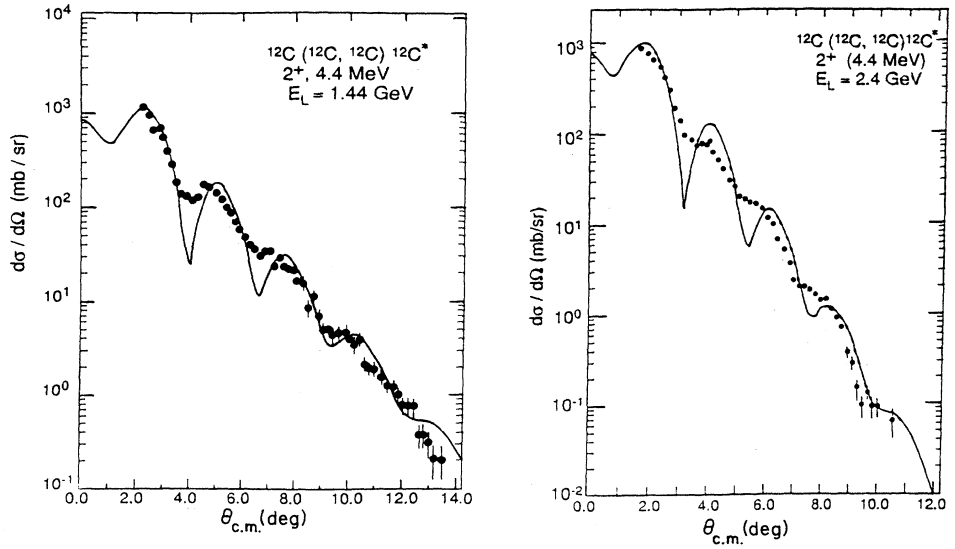

FIG. 11. Angular distributions for ^{12}C inelastic scattering to the 2^+ (4.4 MeV) state of ^{12}C at 1440 and 2400 MeV. The deformation parameter β_2 used is 0.45. The experimental data are taken from Ref. 14.

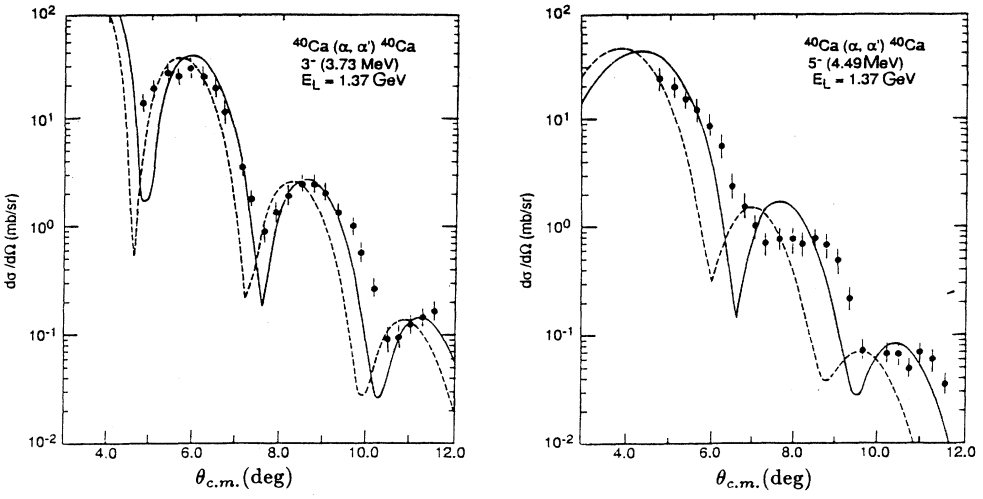

FIG. 12. Inelastic angular distributions of 1.37 GeV α particles exciting the 3^- and 5^- states in ^{40}Ca. Full lines correspond to the transition densities calculated with the "standard" model, while dashed lines correspond to those of the Tassie model. For both the transition densities the deformation parameters are chosen so as to reproduce the experimental $B(E,L)$ values. The experimental data are taken from Ref. 6.

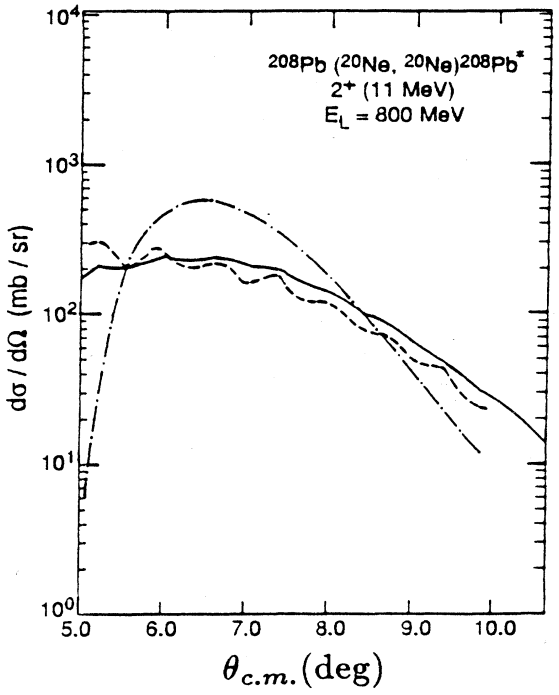

FIG. 13. Partial contributions to the inelastic angular distribution for the inelastic scattering of ^{20}Ne exciting the giant quadrupole resonance of ^{208}Pb at 11 MeV. For the nuclear excitation, the full line corresponds to the Glauber model prediction and the dashed line corresponds to the DWBA results.[23] The dashed-dotted line corresponds to the Coulomb excitation. The deformation parameter β_2 used is 0.085.

agreement with that emerging from the analysis of proton induced inelastic scattering.[16]

In the case of inelastic scattering between heavier ions, where the role of the Coulomb excitation is more important, the model presented here can only account for the contribution of the nuclear excitation. As is stated in Sec. II this is due to the long-range character of the Coulomb force. We cannot therefore in these cases aim at a direct comparison with experimental data. Rather we can compare with a theoretical calculation based on the standard DWBA formalism. In Fig. 13 the different contributions to the inelastic angular distribution for the ^{20}Ne+^{208}Pb reaction exciting the giant quadrupole resonance are displayed. The cross section predicted by the optical limit of the Glauber model compares well with that obtained through a DWBA calculation. This nuclear contribution is however overwhelmed by the Coulomb excitation, also displayed in the figure.

V. CONCLUSIONS

The results obtained within the optical limit to the Glauber model for a large variety of elastic and inelastic collision processes prove the reliability of our method for the analysis of intermediate-energy heavy-ion collisions. Concerning the relation with standard approaches, we emphasize that our results are of comparable quality with respect to those obtained by the DWBA method, in spite of the fact that the former have been obtained without adjusting any parameter. Furthermore, as discussed at the end of Sec. III and in Ref. 3, there exists a tight connection between the potentials used in the standard optical model and the ones obtained through the inversion of the optical-limit phase shift by the Abel transform.

[1]G. R. Satchler, *Direct Nuclear Reactions* (Clarendon Press, Oxford, 1983).
[2]R. M. De Vries and J. C. Peng, Phys. Rev. C **22**, 1055 (1980). J. C. Peng, R. M. DeVries, and N. J. DiGiacomo, Phys. Lett. **98B**, 244 (1981); N. J. DiGiacomo, R. M. DeVries, and J. C. Peng, Phys. Rev. Lett **45**, 527 (1980).
[3]A. Vitturi and F. Zardi, Phys. Rev. C **36**, 1404 (1987).
[4]S. M. Lenzi, A. Vitturi, and F. Zardi, Phys. Rev. C **38**, 2086 (1988); S. M. Lenzi, Vitturi, and F. Zardi, *Proceedings of the Third International Conference on Nucleus Nucleus Collisions, Saint-Malo, 1988,* edited by C. Estère *et al.* (Centre de Publications de l'Université, Caen, 1988), p. 154.
[5]I. Ahmad, J. Phys. G **4**, 1695 (1978).
[6]T. S. Bauer *et al.*, Phys. Rev. C **19**, 1438 (1979).
[7]S. M. Lenzi, A. Vitturi, and F. Zardi, *Proceedings of the XXVII International Winter Meeting on Nuclear Physics, Bormio, 1989,* edited by L. Lori (Università di Milano, Milano, 1989), p. 187.
[8]W. Czyż and L. C. Maximon, Ann. Phys. (N.Y.) **52**, 59 (1969).
[9]J. Formánek, Nucl. Phys. **B12**, 441 (1969).
[10]A. Vitturi and F. Zardi, Lett. Nuovo Cimento **20**, 640 (1977).
[11]P. Di Giacomo *et al.*, Nuovo Cimento A **63**, 321 (1981).
[12]P. J. Karol, Phys. Rev. C **11**, 1203 (1975).
[13]R. D. Vollier and E. Turtschi, Ann. Phys. (N.Y.) **124**, 290 (1980).
[14]J. Y. Hostachy *et al.*, Nucl. Phys. **A490**, 441 (1988).
[15]M. E. Brandan, S. H. Fricke, and K. W. McVoy, Phys. Rev. C **38**, 673 (1988).
[16]G. D. Alkahazov, Yad. Fiz. **47**, 920 (1988) [Sov. J. Nucl. Phys. **47**, 586 (1988)].
[17]A. Chaumeaux *et al.*, Nucl. Phys. **A267**, 413 (1976).
[18]G. D. Alkhazov *et al.*, Nucl. Phys. **A280**, 365 (1977).
[19]M. Buenerd *et al.*, Nucl. Phys. **A424**, 313 (1984).
[20]M. C. Mermaz *et al.*, Z. Phys. A **326**, 353 (1987).
[21]P. Russell-Chomaz *et al.*, Nucl. Phys. **A477**, 345 (1988).
[22]M. Buenerd *et al.*, Phys. Lett. **102B**, 242 (1981).
[23]T. Suomijarvi *et al.*, Nucl. Phys. **A491**, 314 (1989).
[24]C. W. de Jager *et al.*, At. Data Nucl. Data Tables **14**, 479 (1974).
[25]P. C. Barret and D. F. Jackson, *Nuclear Sizes and Structure* (Oxford University Press, New York, 1977).